BEAM DYNAMICS IN THE FRIB LINAC*

R. C. York#, X. Wu, Q. Zhao, M. Doleans+, F. Marti, E. Pozdeyev,
National Superconducting Cyclotron Laboratory, East Lansing, MI 48824, U.S.A.

Abstract

The Facility for Rare Isotope Beams (FRIB), a Department of Energy (DOE) national user facility to provide intense beams of rare isotopes for nuclear science researchers, is currently being established on the campus of Michigan State University (MSU). A superconducting driver linac will deliver cw beams of stable isotopes with an energy of >200 MeV/u at a beam power of 400 kW. Highly charged ions will be produced from an Electron Cyclotron Resonance Ion Source (ECRIS) with a total extraction current of several mA. Multiple charge states of heavier ions will be accelerated simultaneously to meet the final beam power requirement. The FRIB driver linac lattice design has been developed and end-to-end beam simulations have been performed to evaluate the machine performance. An overview of the beam dynamics is presented.

INTRODUCTION

The 2007 Long Range Plan for Nuclear Science had as one of its highest recommendations the "construction of a Facility for Rare Isotope Beams (FRIB) a world-leading facility for the study of nuclear structure, reactions, and astrophysics." [1] FRIB, currently being established on the campus of Michigan State University (MSU) under a Cooperative Agreement between Department of Energy (DOE) and MSU, will be a DOE national user facility providing intense fast, stopped, and re-accelerated beams of rare isotopes for nuclear science researchers to understand the fundamental forces and particles of nature as manifested in nuclear matter, and to provide the necessary expertise and tools from nuclear science to meet national needs. Since the 2008 selection of MSU as the FRIB site, the driver linac layout has been evaluated and the double-folded configuration, as shown in Fig. 1, was chosen as the preferred alternative in 2010. The choice of the driver linac layout was largely driven by goal to reduce overall project cost while maintaining the performance and upgrade potential.

The FRIB facility is based on a superconducting heavy ion linac with >200 MeV/u for all varieties of stable ions at beam power of 400 kW [2]. The uncontrolled beam loss specification for the cw, high power linac is ≤1 W/m to facilitate hands-on maintenance. To meet the beam intensity requirements, the FRIB linac will utilize simultaneous multi-charge-state acceleration for heavier ions. The driver linac will consist of a Front End to bring the beam energy to 0.3 MeV/u, three superconducting acceleration segments connected by two 180° bending systems to achieve a final beam energy of >200 MeV/u and a Beam Delivery System to transport the multi-charge-state beams to a fragmentation target, as shown in Fig. 1. The superconducting linac has an 80.5 MHz base frequency and utilizes four types of resonators with only one frequency transition to 322 MHz after the Linac Segment 1 of Fig. 1.

Several codes were used to design the driver linac lattice. The transport and matching in the Front End, the two 180° bending sections and the Beam Delivery System were performed using DIMAD, COSY and TRACE3D. The superconducting linac lattice was optimized for multiple charge state acceleration using a code developed at MSU. End-to-end beam simulations with high statistics have been performed using the code RIAPMTQ and IMPACT on high-performance parallel computers.

LINAC LATTICE DESIGN

The FRIB driver linac lattice design has been developed and evaluated through several evolutions [3,4]. The double-folded geometry was chosen to reduce overall project cost, and the beam dynamics of that design is discussed here.

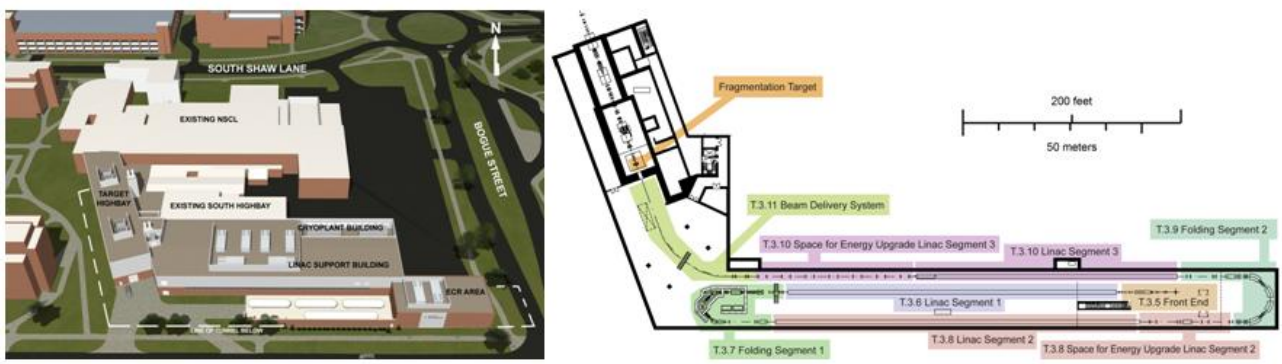

Figure 1: The planned FRIB surface buildings (left) and the layout of the double-folded superconducting driver linac in tunnel (right).

* Work supported by US DOE Cooperative Agreement DE-SC000661
# york@frib.msu.edu + now at ORNL, Oak Ridge, TN 37831, USA

Even a state-of-the-art ECRIS is unable for heavier ions (above xenon) to produce sufficient beam current in a single charge state to satisfy the 400 kW beam power requirement. Therefore, for heavier ions two charge states are selected from the ECRIS. The Low Energy Beam Transport (LEBT) [5] matches beam from the ECRIS into a Radio Frequency Quadruple (RFQ).

The RFQ cell design was accomplished using the PARMTEQ code package. To achieve the smallest longitudinal emittance from the RFQ, the beam is externally bunched in the LEBT. The RFQ was designed to have a reduced longitudinal acceptance so as to capture fewer particles at the extremes of the distribution. Following a transition cell, a radial matching section was also employed at the exit to produce an axial-symmetric output beam for the solenoid focusing in the downstream Medium Energy Beam Transport (MEBT). More information on the RFQ design can be found in reference [6]. To achieve the matched beam parameters at the entrance of the first superconducting linac (Linac Segment 1) and to provide flexible matching for different ions, the MEBT includes two room temperature rf bunchers and three superconducting solenoids.

The first superconducting linac (Linac Segment 1 in Fig. 1) will consist of two types of cryomodules with two types of quarter wave resonators (QWRs) both operating at 80.5 MHz [7]. A schematic layout of the two types of cryomodules is shown in Fig. 2. Four cryomodules each containing four β_{opt}=0.041 QWRs and two superconducting solenoids will bring the beam energy from 0.3 MeV/u to ~1.4 MeV/u followed by twelve cryomodules each containing eight β_{opt}=0.085 QWRs and three superconducting solenoids to accelerate the beam to ~17 MeV/u at the end of Linac Segment 1. Each superconducting solenoid has a pair of dipole windings to provide the central orbit correction due to lattice alignment errors. Energy gain per accelerating gap of the QWRs (with two gaps) for a beam of A/Q=7 is shown in Fig. 3. The Linac Segment 1 lattice was optimized to simultaneously accelerate two-charge-state beams. Due to the high accelerating voltage of the β_{opt}=0.041 QWRs (with respect to the input beam energy), the voltages of the QWRs were gradually increased from ~40% of the nominal value in the first two cryomodules with a synchronous phase of about -35° to balance the longitudinal phase advance and acceptance. The last two β_{opt}=0.041 QWRs were adjusted to provide longitudinal matching into the downstream β_{opt}=0.085 cryomodules. Fig. 3 also shows from particle tracking the longitudinal acceptance of Linac Segment 1. The longitudinal acceptance to emittance ratio is ~10.

Folding Segment 1 of Fig. 1 includes a charge stripping system to increase the beam charge state and a bending system to provide a compact geometry. A rebuncher cryomodule with two β_{opt}=0.29 half wave resonators (HWRs) together with the last cavity in the last cryomodule of Linac Segment 1 are used for longitudinal matching while quadrupoles provide transverse matching onto stripper to minimize beam emittance growth due to interaction with the stripping material. The mean charge state of a uranium beam will at a stripping energy of 16.6 MeV/u increase from 33.5 (33+ and 34+) to 78 assuming a solid stripper. Five charge states (76+ to 80+) of uranium beam are then selected and transported through a 180°, second-order achromatic magnetic bending section to limit the multi-charge-state beam emittance growth. A cryomodule of two β_{opt}=0.085 QWRs right after the bend and a cryomodule of two β_{opt}=0.29 HWRs before Linac Segment 2 are used to match the beam longitudinally from stripper into the entrance of Linac Segment 2.

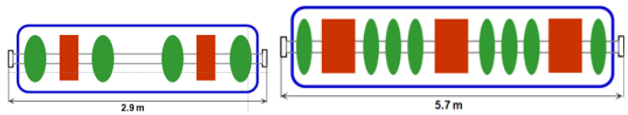

Figure 2: Schematic layout of the two types of cryomodules in Linac Segment 1: (Left) β_{opt}=0.041 QWRs in green and (Right) β_{opt}=0.085 QWRs in green. Solenoids are in red.

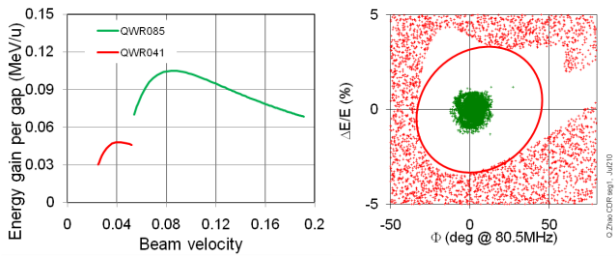

Figure 3: (Left) Energy gain per accelerating gap (QWRs have two gaps) for a beam of A/Q=7; (Right) Longitudinal acceptance (area within red ellipse) of Linac Segment 1 together with the tracked particles of a two-charge-state input beam (green).

Linac Segment 2 consists of two types of cryomodules with two types of HWRs both operating at 322 MHz [8]. The schematic layout of the two types of cryomodules is shown in Fig. 4. Thirteen cryomodules each containing six β_{opt}=0.29 HWRs accelerate beam energy from 16.4 MeV/u to ~55 MeV/u followed by seven cryomodules each containing eight β_{opt}=0.53 HWRs to bring the beam to ~105 MeV/u. Both cryomodule types have one superconducting solenoid with a pair of dipole windings for misalignment correction. Energy gain per accelerating gap of the HWRs (two gaps) for a beam of A/Q=3 is shown in Fig. 5. The Segment 2 lattice is optimized to simultaneously accelerate a five-charge-state beam. Several solenoids were adjusted to provide transverse matching between the two types of cryomodules. To achieve a large longitudinal acceptance in Linac Segment 2, the synchronous phase was kept at about -35° for the β_{opt}=0.29 HWRs and -25° for the β_{opt}=0.53 HWRs. Fig. 5 also shows the longitudinal acceptance of Linac Segment 2 together with the results of particle tracking. The longitudinal acceptance to emittance ratio of Linac Segment 2 is ~20.

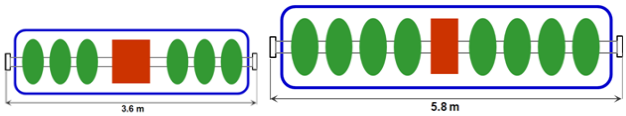

Figure 4: Schematic layout of the two types of cryomodules in Linac Segment 2: (Left) β_{opt}=0.29 HWRs in green and (Right) β_{opt}=0.53 HWRs in green. Solenoids are in red.

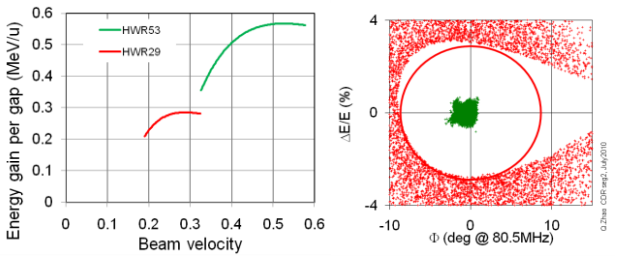

Figure 5: (Left) Energy gain per accelerating gap (HWRs have two gaps) for a beam of A/Q=3; (Right) Longitudinal acceptance (area within red ellipse) of Linac Segment 2 together with the tracking results of a five-charge-state beam (green).

The design philosophy of the 2nd 180° bending system (Folding Segment 2 in Fig. 1) is similar to that for Folding Segment 1. Linac Segment 3 consists of eleven β_{opt}=0.53 HWR cryomodules of the same layout as those in Linac Segment 2 bringing the final beam energy >200 MeV/u. The longitudinal acceptance to emittance ratio of Linac Segment 3 is ~40. The Beam Delivery System is designed to transport a multi-charge-state beam to a fragmentation target with ~90% of the beam within a diameter of ~1 mm. The Beam Delivery System has a 70° achromatic bending section with high-order corrections to minimize multi-charge-state beam emittance growth.

END-TO-END BEAM SIMULATIONS

Beam simulation-based studies have been essential to the evaluation and optimization of the FRIB linac lattice performance. Since the uranium beam with its multi-charge-states is the most challenging, results will be presented for this beam.

Based on available experimental data, a normalized transverse rms emittance of 0.1 π-mm-mrad was assumed after ECRIS charge state selection as well as an intrinsic energy spread of ±0.05%. A total of one million particles ($^{238}U^{33+}$ and $^{238}U^{34+}$) were tracked from the entrance of the LEBT, through the RFQ, MEBT, Linac Segment 1, Folding Segment 1 including the charge stripper, Linac Segment 2, Folding Segment 2, Linac Segment 3, and Beam Delivery System to the fragmentation target. A stripper medium with an effective thickness of 3 micrometer was modeled in the beam simulation assuming a thickness variation of ±10%. Fig. 6 shows the evolution of the beam energy and beam envelope for a multi-charge-state uranium beam from the exit of the RFQ to the fragmentation target.

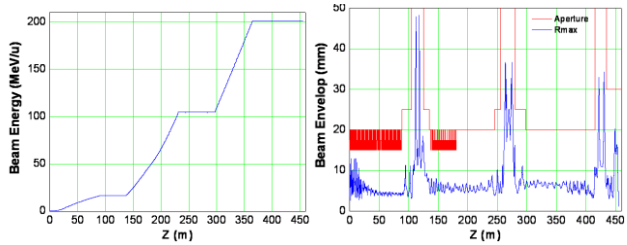

Figure 6: (Left) Evolution of beam energy and (Right) beam envelope for a multi-charge-state uranium beam from the exit of the RFQ to the fragmentation target.

Even for a machine without errors (rf fluctuations or misalignments) simulations show an increase in both the transverse and longitudinal emittance because of the multiple-charge states, passage through the stripping medium, and magnetic aberrations of the two Folding Segments. For example, the normalized transverse and longitudinal 99.99% emittance (defined as an emittance enclosing 99.99% of ~1 million particles based on the rms Twiss parameters) of a two-charge-state uranium beam at injection into the Linac Segment 1 are 1.4 π-mm-mrad and 3.1 π-keV/u-ns, respectively. The effective five-charge transverse emittance (see Fig. 7) at the end of Linac Segment 3 is approximately 2.6 π-mm-mrad largely due to chromatic (Q/A differences between charge states) effects since the emittance of each individual charge state increased by only about 15%. The longitudinal emittance growth was mitigated by making the longitudinal acceptance as large as possible so that the beam would primarily be in the linear region of the acceptance. The effective five-charge state longitudinal emittance (see Fig. 7) at the exit of the driver linac is about 33 π-keV/u-ns largely due to the differing phase space motion of each charge state since the emittance growth of each individual charge state is about 5 times less. The corresponding rms emittances are about one order of magnitude smaller. The phase space distributions of tracked particles at the entrance of Linac Segment 1, after the stripper, at the exit of Linac Segment 2, and on the fragmentation target are presented in Fig. 7. As shown in Fig. 8, at the fragmentation target ~90% of the five-charge-state uranium beam ($^{238}U^{76+}$ to $^{238}U^{80+}$) is within a 1 mm diameter of beam size meeting a requirement of the Fragmentation Separator.

To estimate the performance of the linac under more realistic conditions, beam simulations including machine imperfections were carried out. A total of 120 different seeds were used for the multi-charge-state uranium beam with rf errors specified in Table 1. For each seed, one million particles were tracked from the exit of the RFQ through the three Linac Segments and two Folding Segments to the exit of linac. The transverse rms emittance of the multi-charge-state uranium beam at the exit of linac was found to increase by ~10% due to the rf errors showing little coupling between the transverse and longitudinal. The longitudinal rms emittance of multi-charge state uranium beam was found to increase about

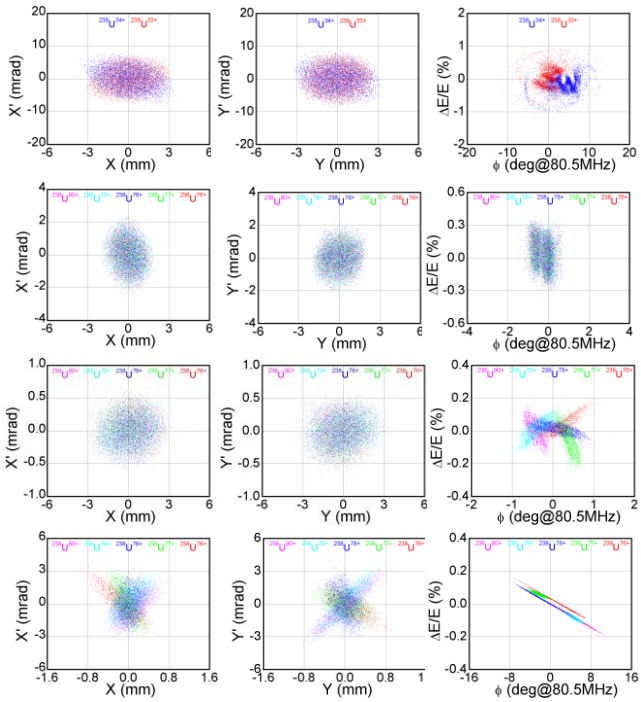

Figure 7: Phase space plots from end-to-end simulations of a multi-charge-state uranium beam at the entrance of Linac Segment 1 (Top row), after stripper (2nd row), at the exit of Linac Segment 2 (3rd row), and at the fragmentation target (Bottom row).

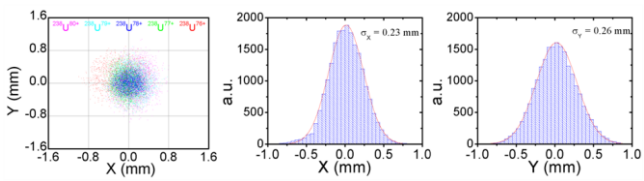

Figure 8: Distribution of five-charge-state uranium beam at the fragmentation target in xy plane (left), and projections in the horizontal (middle) and vertical (right) planes with σ values corresponding to the Gaussian fit in red. ~90% of the beam is within 1 mm diameter size.

4.5 times due to the rf errors demonstrating an expected sensitivity to rf variations. Fig. 9 shows an example of the longitudinal phase space of a two-charge-state uranium beam before the stripper without rf errors and with errors double those specified in Table 1. Although the two charge states are superimposed for the case of no errors, they are sufficiently separated for larger rf errors (twice Table 1 values) that simulations showed beam loss.

Table 1: Superconducting Cavities rf Fluctuation Limits

Name	Tolerance	Distribution
rf amplitude error	±1.5% (truncated at 3σ)	Gaussian (σ=0.5%)
rf phase error	±1.5° (truncated at 3σ)	Gaussian (σ =0.5°)

The longitudinal emittance growth produced by the rf errors as specified in Table 1 was found to be acceptable for the driver linac. With these errors, even for the challenging case of a multiple-charge-state uranium beam, the results of end-to-end simulations show that the emittance remains well within the linac longitudinal acceptance and that the transverse beam envelope growth is small.

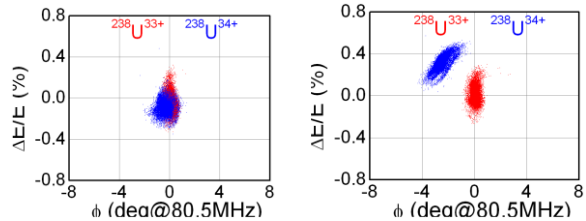

Figure 9: Longitudinal phase space of a two-charge-state uranium beam (33+ in red, 34+ in blue) before stripper (Left) without rf errors and (Right) with rf errors double those specified in Table 1.

The evaluation of the effect of misalignment combined with rf errors has not been completed for the double-folded lattice. However, the evaluation results of our previous lattices with the same alignment errors show that misalignment mainly affects the transverse plane and does not couple into the longitudinal plane [4]. Beam envelope growth due to misalignment is typically within ~5 mm still remaining well within the apertures. The end-to-end beam simulations indicate that the driver linac will have adequate acceptances, even for acceleration of the multiple-charge-state uranium beam.

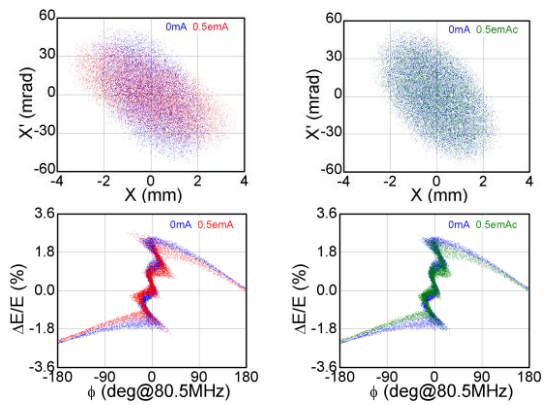

Figure 10: Horizontal (Top) and longitudinal (Bottom) phase space of uranium beam at the entrance of the RFQ without (blue), with 0.5 emA space charge effects (red on left), and with compensation (green on right).

SPACE CHARGE EFFECTS

For a multi-component, high current (several mA) beam extracted from the ECRIS, space charge effects will have a significant impact on the transverse beam dynamics [5], though space charge neutralization may play an important role. However, for heavy ions after charge selection, the typical beam has an electrical current of ~0.5 emA with a beam energy of 12 keV/u, and therefore space charge effects are insignificant. As an example, Fig. 10 shows the horizontal and longitudinal phase space of a uranium beam at the entrance of the RFQ without and with (0.5 emA) space charge effects. The space charge effects can be compensated by increasing the

focusing strength and buncher voltages by only ~1%. For light ions, such as proton, space charge effects will be important even after charge selection. In this case, we plan to inject molecules (e.g. use H_3^+ instead of protons) [6] to mitigate space charge effects.

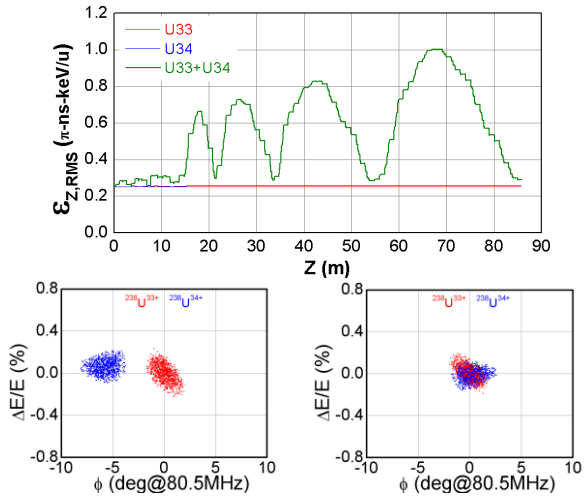

Figure 11: (Top) Longitudinal rms emittance of two-charge-state uranium beam along Linac Segment 1 with charge state 33+ in red, 34+ in blue, and two-charge-state (33+ & 34+) in green; (Bottom-left) longitudinal phase space of uranium beam (33+ in red, 34+ in blue) at ~68 m along Segment 1 where the two charge states are the most separated due to the longitudinal oscillation, and (Bottom-right) at the exit of Linac Segment 1 where they overlap.

MULTI-CHARGE-STATE ACCELERATION

A substantial challenge for the linac beam dynamics design is the simultaneous multi-charge-state acceleration of heavy ions necessary to meet the beam power requirement. Beam mismatch amongst the different charge states leads to a larger effective emittance in both transverse and longitudinal planes. For example the chromatic effects must be compensated to achieve a five-charge-state beam focus to obtain the required 90% of the beam with a 1 mm beam spot at the fragmentation target as shown in Fig. 8. To mitigate the effects of beam passage through the stripper medium, the two charge-state beam from Linac Segment 1 must have at the stripper a minimum focus in the longitudinal as well as transverse planes. Fig. 11 shows the longitudinal rms emittance of the two-charge-state uranium beam along Linac Segment 1. For each single charge state (33+ or 34+), there is no longitudinal emittance growth. However, the longitudinal emittance of the two-charge-state beam oscillates and can effectively reach five times larger. The longitudinal oscillation frequency (f_{lo}) is determined by [9]

$$f_{lo} = f\sqrt{\frac{qE_oT\lambda\sin(-\phi_s)}{2\pi mc^2\gamma_s^3\beta_s}} \qquad (1)$$

where f is the cavity rf frequency, q is the charge, E_o is the average axial electric field, T is the transit-time factor, λ is the rf wavelength, ϕ_s is the synchronous phase, mc^2 is the rest energy, γ_s and β_s are the relativistic energy and velocity of the synchronous particle, respectively. Thus, the oscillation period gets longer as the beam velocity increases as shown in Fig. 11. Since different charges have different longitudinal oscillation periods, the centroids and the Twiss parameters of the different charge states in the longitudinal phase space vary throughout the linac. Effective emittance is larger when two charge states are separated, and becomes smaller when they come close, as shown in the phase space plots of Fig. 11.

The driver linac must also accommodate two-charge-state acceleration for other ions heavier than xenon. To obtain the proper longitudinal oscillations so as to achieve a minimum emittance at the stripper, individual cavity synchronous phases will be adjusted for different ions (different $\Delta Q/Q_o$). Fig. 12 shows longitudinal rms emittances of a two-charge-state xenon beam ($^{136}Xe^{19+}$ and $^{136}Xe^{20+}$) along Segment 1. With the same phase settings as those of uranium, the two charge states of xenon beam reach a maximum separation at the exit of Segment 1. Adjustment of the synchronous phases by ~5° was sufficient to achieve the minimum emittance.

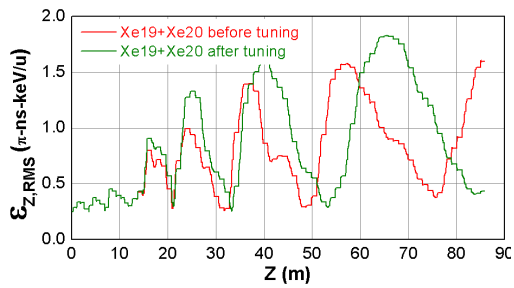

Figure 12: Longitudinal rms emittances of two-charge-state (19+ & 20+) xenon beam along Linac Segment 1 with the rf phases for a uranium beam (red) and with xenon phase setting (green) adjusted to bring the charge states together at the stripper.

CONCLUSION

Extensive beam dynamics simulation studies have demonstrated that the FRIB linac design will meet performance requirements with simultaneous multi-charge-state acceleration required to meet the beam power specification.

REFERENCES

[1] http://www.er.doe.gov/np/nsac/docs/ Nuclear-Science.Low-Res.pdf.
[2] R.C. York, et al., SRF'09, p888; http://www.jacow.org.
[3] X. Wu, et al., Linac'04, p594; Q. Zhao, et al., Linac'06, p457; Q. Zhao, et al., PAC'07, p1775; http://www.jacow.org.
[4] Q. Zhao, et al., PAC'09; http://www.jacow.org.
[5] Q. Zhao, et al., AIP Conf. Proc. 749(2005)242.
[6] Q. Zhao, et al., Linac'04, p599; http://www.jacow.org.
[7] W. Hartung, et al., SRF'09, p201; http://www.jacow.org.
[8] W. Hartung, et al. PAC'11, to be published.
[9] T.P. Wangler, RF Linear Accelerators, 2nd edition, Wiley-Vch (Weinheim), 2008, p.186.